Check for updates

DR. DEBORAH STROKA (Orcid ID : 0000-0002-3517-3871)

Received Date : 07-Dec-2021

Revised Date : 31-Mar-2022

Accepted Date : 11-Apr-2022

Article type : Research Article

LIM protein Ajuba promotes liver cell proliferation through its involvement in DNA replication and DNA damage control

Noëlle Dommann, Jacopo Gavini, Daniel Sánchez-Taltavull, Felix Alexander Baier, Fabienne Birrer, Giulio Loforese, Daniel Candinas, Deborah Stroka

Department of Visceral Surgery and Medicine, University of Bern, Inselspital, Bern University Hospital, Switzerland

Correspondence: deborah.stroka@dbmr.unibe.ch; Tel.: +41 31 632 27 48

Abbreviations

CCl_4 carbon tetrachloride

CDC6 cell division cycle 6

This article has been accepted for publication and undergone full peer review but has not been through the copyediting, typesetting, pagination and proofreading process, which may lead to differences between this version and the Version of Record. Please cite this article as doi: 10.1002/1873-3468.14371

This article is protected by copyright. All rights reserved

Accepted Article

DEN diethylnitrosamine
EdU 5-ethynyl-2′-deoxyuridine
ESCC esophageal squamous cell carcinoma
HCC hepatocellular carcinoma
HUVEC human umbilical vascular endothelial cells
MCM mini-chromosome maintenance
ORC origin recognition complex subunit 1
ORI origins of replication
PHx partial hepatectomy
PMA phorbol 12-myristate 13-acetate
RPA replication binding protein A
sh short hairpin

Abstract

The LIM-domain protein Ajuba is associated with cell proliferation, a fundamental process of tissue regeneration and cancer. We report that in the liver, Ajuba expression is increased during regeneration and in tumor cells and tissues. Knockout of Ajuba using CRISPR/Cas9 is embryonic lethal in mice. shRNA targeting of Ajuba reduces cell proliferation, delays cell entry into S-phase, reduces cell survival and tumor growth *in vivo*, and increases expression of the DNA damage marker γH2AX. Ajuba binding partners include proteins involved in DNA replication and damage, such as SKP2, MCM2, MCM7 and RPA70. Taken together, our data support that Ajuba promotes liver cell proliferation associated with development, regeneration, and tumor growth and is involved in DNA replication and damage repair.

This article is protected by copyright. All rights reserved

Introduction

Cell proliferation is the fundamental process needed for cell renewal, wound repair and tissue regeneration and is dependent on the tightly controlled process of DNA replication[1,2]. However, cell proliferation is increased in malignant cells with the difference between healthy and tumor cell proliferation being the loss of control in malignant cells over the process[3,4]. DNA replication begins at origins of replication (ORI) located throughout the genome and ORI licensing occurs during S-phase of cell cycle when the pre-replication complex is assembled[5]. The pre-replication complex is formed by proteins such as origin recognition complex subunit 1 (ORC), mini-chromosome maintenance (MCM2-7) and cell division cycle 6 (CDC6).

Ajuba is a LIM domain protein described as an adaptor protein by linking and modulating different members of functional complexes[6]. Ajuba contains a nuclear export sequence, enabling it to translocate from the cytoplasm to the nucleus and 3 tandem LIM motifs in its C terminus[7-10]. Ajuba is a versatile scaffold protein associated with numerous protein complexes and among the best characterized function of Ajuba is its role in stabilizing cell-cell junctions by direct binding to F-and α-tubulin[11,12].

Ajuba has been described to be involved in several proliferation pathways such as the Hippo and Wnt signaling pathways and in the ATR-mediated DNA damage response pathway[13,14,15]. It has also been found to be dysregulated in cancer[13,16,17,18]. Ajuba was found to be significantly upregulated in colorectal cancer, esophageal squamous cell carcinoma and cervical cancer[17,19,20,21]. However, its reported function in cancer is contradictory. There are which describe Ajuba as a driver of tumor cell proliferation[19-26], whereas in others, it is described as a tumor suppressor and an inhibitor of proliferation[27-29]. Additionally, Ajuba was found to be mutated in cutaneous and esophageal squamous cell carcinoma (ESCC)[16-18,25,30]. Non-silent Ajuba mutations were found in 3.9% of a 490 ESCC tumor cohort. Tumors with mutations in Ajuba had lower Ajuba expression and significantly better patient survival when compared to tumor samples with non-mutated Ajuba expression[30].

Thus far, the role of Ajuba in liver cancer has been investigate in three publications resulting in contradictory conclusions. Two reports describe Ajuba as a driver of hepatocellular carcinoma (HCC) cell proliferation[6,31], whereas one paper describes Ajuba as a tumor suppressor and inhibitor of cell growth in HCC[28]. We were therefore convinced that elucidating the role and mechanism of

This article is protected by copyright. All rights reserved

how Ajuba is involved in proliferation in the liver in both healthy and regenerating cells and in liver tumor cells is crucial. Therefore, in this study we investigated the role of Ajuba in HCC and in regenerating liver tissue, focusing on its role in cell proliferation.

Results

2.1 Ajuba expression coincides with cell proliferation in normal and malignant liver cells

We first questioned if Ajuba expression is increased when cells transition from a quiescent to a proliferative state using the well-established model of partial hepatectomy (PHx)[1]. Following PHx, liver cells are synchronized to enter cell cycle and replicate to replace the lost tissue. Ajuba mRNA increased 24 to 48h following PHx (Figure 1A). Ajuba protein expression increased and coincided with hepatocyte proliferation[32] occurring 48 to 72 hours post PHx (Supplementary Figure 1). Next, we induced regenerative proliferation by damaging the liver with carbon tetrachloride (CCl_4) and diethylnitrosamine (DEN)[33, 34] and Ajuba mRNA was significantly increased in the damaged liver tissues (Figure 1B). Ajuba mRNA and protein expression were higher in proliferating malignant liver cancer cell lines when compared to non-proliferating hepatocytes in culture (Figure 1C and Supplementary Figure 2). We next questioned if Ajuba expression is modulated when cells transition from a proliferative to a differentiated or a cell cycle arrested state. The monocyte cell line U937 was differentiated to mature macrophage-like cells with phorbol 12-myristate 13-acetate (PMA)[35,36] or treated with nocodazole to arrest cell growth in the G2 phase of cell cycle[27,37]. Both conditions blocking cell proliferation resulted in significantly lower Ajuba mRNA levels (Supplementary Figure 3). We next used lentiviral transduction of an Ajuba expression construct to demonstrate that Ajuba overexpressed in Huh7 HCC cells leads to an increase in proliferation compared to the parental and shScrambled controls (Figure 1D). In human livers samples containing HCC tumors, we dissected tumor and adjacent non-tumor tissues and measured an increased expression of Ajuba mRNA compared to normal hepatocytes (Figure 1E). Also, Ajuba mRNA was highly expressed in human HCC organoids, which were actively proliferating as shown by immunofluorescence of positive 5-ethynyl-2′-deoxyuridine (EdU) incorporation[38] (Figure 1E and Supplementary Figure 4). Furthermore, we consulted The Cancer Genome Atlas[39]

This article is protected by copyright. All rights reserved

and plotted Kaplan Meyer curves to determine HCC patient survival with high vs. low Ajuba expression. High expression of Ajuba correlated with a decrease in HCC patient survival (Figure 1F). Taken together, our data demonstrates that Ajuba expression coincides with cell proliferation in both normal and malignant liver tissues and high tumor expression of Ajuba is correlated with decreased HCC patient survival.

2.2 Loss of Ajuba expression leads to decreased cell proliferation.

Based on our observations that proliferating cells were associated with increased Ajuba expression, we wanted to investigate if Ajuba was necessary for cell proliferation, particularly in physiological processes like liver regeneration and hepatocarcinogenesis. Therefore, we attempted to generate an Ajuba KO mouse line using CRISPR/CAS9 and pronuclear injection (Supplementary Figure 5a-d). However, following extensive breeding and genotyping, we were unable to generate a homozygous Ajuba KO mouse line (Figure 2A, n=400). We performed timed matings and in vitro fertilization to genotype embryos and blastocysts respectively. After again only obtaining WT and heterozygous KO mice, we concluded that the homozygous Ajuba KO mice were embryonically lethal (Supplementary Figure 5e-f). This result was supported by our parallel observation that full loss of Ajuba using CRISPR/Cas9 KO in the RIL-175 mouse HCC cell line lead to non-proliferating and non-viable clones[40]. Failing to generate a knock-out mouse or cell lines, we switched to study loss of Ajuba expression using lentiviral transduction of short hairpin (sh)RNAs. We modulated Ajuba expression in the human Huh7 cells using 2 lentiviral constructs targeting a coding (shAjuba1) and non-coding (shAjuba2) region of Ajuba. We observed a significant decrease of Ajuba mRNA and protein compared to the shScrambled control (Figure 2B and Supplementary Figure 6). We next performed several biological assays in vitro and in vivo. Using an MTT assay to assess cell proliferation, we observed that proliferation was significantly decreased in Huh7 cells with knocked down Ajuba expression (Figure 2C). Moreover, Huh7 cells with loss of Ajuba expression had a significantly decreased ability for colony formation (Figure 2D). The loss of cell growth in vitro was also confirmed in vivo using the syngeneic tumor model, RIL-175 mouse HCC cells in C57Bl/6 mice. After 11 days, tumor volumes were significantly decreased in cells transduced with the shRNA targeting the coding region of Ajuba (shAjuba1) and a trend of smaller

This article is protected by copyright. All rights reserved

tumors was observed in shAjuba2 shRNA targeting the non-coding region (Figure 2E and Supplementary Figure 7). To give further evidence of the biological importance of Ajuba in normal cells, we assessed the impact of loss of Ajuba expression in human umbilical vascular endothelial cells (HUVEC). In a tube formation assay[41], loss of Ajuba expression decreased total vessel length thereby suggesting its importance in the process of angiogenesis (Figure 2F). Taken together our data indicate that Ajuba is necessary for proliferation in liver tumor cells, in normal endothelial cells and for embryonic development.

2.3 Ajuba has a nuclear localization in proliferating cells and involved in DNA replication

Supporting a role of Ajuba in proliferation, we could demonstrate by immunohistochemistry the nuclear localization of Ajuba in proliferating HCC tumor and regenerating liver tissues (Figure 3A). The effect of altered Ajuba expression on DNA replication and S-phase entry was monitored over a 24-hour period. Ajuba KD, OE and control cell lines were synchronized using thymidine, a DNA synthesis inhibitor that arrests cell cycle at the G1/S boundary[42,43]. The arrested cells were then released with complete medium containing 25uM EdU to label the cells entering cell cycle[44]. Ajuba KD cell lines had a significant decreased EdU incorporation and a delay in S-phase entry (Figure 3B). Delayed S-phase entry is shown by the altered slope of shAjuba1 looking at the y-intercept/2 of the linear regression. The Ajuba overexpressing (OE) cell line, however, showed the highest percentage of EdU incorporation and seem to be the quickest cells to start DNA replication. We next investigated how Ajuba may be involved in proliferation by checking the expression of genes known to be involved in the regulation of cell cycle using the RT2 Qiagen microarray composed of cell cycle genes in liver cancer cell line Huh7. In both cell lines with loss of Ajuba expression, we observed reduced expression of genes associated with the initiation of DNA replication, such as S-phase kinase associated protein 2 (*SKP2)*, *MCM2* and *MCM3*, E2F transcription factor 4 (*E2F4)* and *CDC6* genes (Figure 3C).

2.4 Ajuba is associated with DNA replication genes

This article is protected by copyright. All rights reserved

To further understand the mechanistic role of Ajuba in proliferation, we next sought to identify interacting protein partners of Ajuba. We used an Ajuba OE cell line with an HA-tag present in the construct to pull down the Ajuba protein followed by mass spectrometry to identify the proteins binding to Ajuba (Figure 4A). The Ajuba scrambled control plasmid, containing a scrambled sequence and no HA-tag, was used to account for unspecific binding. We identified 1072 proteins of which 165 proteins were detected uniquely in the Ajuba OE samples (Class I) and 673 proteins that were higher expressed in Ajuba OE compared to the control (log 2-fold change) (Figure 4B and 4C). Supplementary Figure 8A displays a string analysis of proteins detected by mass spectrometry that were uniquely or preferentially present in Ajuba OE samples. Several of previously known interaction partners of Ajuba as listed on BioGRIND[45], such as large tumor suppressor kinase 1 (LATS1), tyrosine 3-monooxygenase/tryptophan 5-monooxygenase activation protein zeta (YWHAZ) and aurora kinase B (AURKB), as well as new potential interaction partners were found. Using the proteins displayed in Supplementary Figure 8B, a Metascape pathway enrichment analysis was performed and among those identified, several pathways in which Ajuba is known to be involved, such as the Hippo pathway, apoptosis and tight junctions, were present[7,10,12,23,46]. Additionally, we found potential binding partners of Ajuba to be involved in cell cycle regulation, G2/M checkpoint, Chk1 mediated inactivation of cyclin B and response to DNA damage (Figure 4D). We also detected the presence of several proteins involved in translation initiation, RNA splicing and stability as well as transport. Interestingly potential binding partners were found in various cellular compartments such as the cell-cell junctions, cytoplasm, nuclear as well as mitochondrion and ribosome (Supplementary Figure 9). Looking at the pathway enrichment of Class I and Class II separately, proteins involved in protein localization to nucleus and synthesis of DNA and DNA translation pathways as well as S-phase and cell cycle checkpoints and Chk1/Chk2 mediated response were present (Supplementary Figure 10). To validate our findings that Ajuba has a direct interaction with proteins involved in cell cycle, DNA replication and DNA damage we performed immunoprecipitation experiment and could demonstrate that Ajuba binding partner include replication binding protein A (RPA) subunit 70 (RPA70), SKP2, MCM2, MCM7 (Figure 4E).

2.5 Ajuba depletion leads to increased DNA damage expression

This article is protected by copyright. All rights reserved

As several potential interaction partners of Ajuba were found to be involved in pathways involved in the DNA damage response, we questioned if defects in proliferation are due to an increase of DNA damage with a loss of Ajuba expression. We observed an increase of DNA damage in cells with loss of Ajuba expression already at the steady state level as shown by the increase of the DNA damage marker γH2AX by immunocytochemistry (Figure 5A), by FACS (Figure 5B) and by immunoblot (Figure 5C). Coinciding with γH2AX, we detected an increase of RPA70 which binds to single stranded DNA and sites of DNA damage[47,48] (Figure 5D). The loss of Ajuba also resulted in the cells being significantly more sensitive to DNA damage induced by irradiation (Figure 5E). Sensitivity to irradiation was tested by irradiating the cell lines at different dosages ranging from 0-6 Gray and measuring recovery by colony formation to determine the percentage of survival (Supplementary Figure 11). Lastly, we tested the efficiency of DNA damage repair and compared the percentage of DNA repair occurring between two timepoints, 2h and 4h post irradiation. The scrambled control cells showed the highest percentage of DNA damage repair whereas both cell line with loss of Ajuba expression displayed a lower of DNA damage repair from 2h to 4h post irradiation (Figure 6F and Supplementary Figure 12A).

Discussion

In previous publications, Ajuba has been linked to proliferation however, its role was unclear as it was described as both a driver[19-26] and inhibitor of cell proliferation[27-29]. In our study, we provide convincing evidence that particularly in liver cells, Ajuba is important in proliferation in both malignant and normal cells and tissues. We found Ajuba to be significantly increased in actively proliferating normal and malignant liver cells and tissues. It was significantly upregulated in hepatocyte compensatory proliferation in models of PHx and during damage repair response following damage due to toxin exposure. Ajuba was also found to be significantly more expressed in proliferating liver cancer cells, as well as in human HCC tumors and HCC organoids. Moreover, when monocytic cells switch from a proliferative to a differentiated state, Ajuba expression was reduced. Previous data from our lab demonstrated that knock out of Ajuba using CRISPR/Cas9

This article is protected by copyright. All rights reserved

Accepted Article

resulted in non-viable HCC cell lines[40]. This observation, together with the embryonic lethality of CRISPR/Cas9 KO animals has also been supported by Loganathan et al.[49], and that Ajuba expression was found during embryogenesis in all embryonic germ layers and within fetal components of the developing placenta[50,51]. However, these findings contradict the report in which Ajuba KO mice were reported to have a mild phenotype[52].

Since CRISPR/Cas9 KO of Ajuba led to non-viable clones, we chose to study Ajuba function using lentiviral transduction of shRNAs to knock down its expression. With loss of Ajuba expression, we observed that the proliferation rate of HCC tumor cells was decreased in vitro, and syngeneic tumors had smaller volumes in vivo. With publicly available data from The Cancer Genome Atlas, we found a correlation of high Ajuba expression with poor HCC patient survival, which support the data of Zhang et al., showing that Ajuba expression is related to a more aggressive malignancy and adverse clinical outcome[6].

We found that cells with loss of Ajuba expression have lower levels of *SKP2*, *MCM2*, *MCM3*, *E2F4* and *CDC6*, all genes involved in the initiation of DNA replication. To provide further evidence that Ajuba could be involved directly in the DNA replication complexes, we identified direct interaction partners by MS and co-IP using an Ajuba OE cell line. We identified several potential binding partners of Ajuba were found to be involved in DNA replication and cell cycle control and checkpoints, all pathways with proteins localized in the nucleus. We could confirm that Ajuba is indeed expressed in the nuclear compartment proliferating cells and tissues[53,7] which is also supported by studies showing that Ajuba can be translocated between the cytoplasm and the nucleus[10].

Several of the genes found to be differentially expressed after Ajuba KD as well as proteins identified as potential interaction partners of Ajuba seemed to be involved in DNA replication and more precisely to the pre-replication complex. We therefore decided to take a closer look at the very beginning of DNA replication during the S-phase of cell cycle by assessing if the S-phase entry of the cells with loss of Ajuba expression is affected. We found Ajuba KD cells to have not only a less efficient DNA replication as shown by the decreased percentages of cells being positive for EdU but also a delay of S-phase entry. This could be because the Ajuba depleted cells had less

This article is protected by copyright. All rights reserved

SKP2, MCM2, MCM3 and CDC6 and therefore had problems efficiently licensing the ORI leading to less efficient DNA replication. A reduction of some MCM proteins in human cancer cells causes a rapid increase in the level of DNA damage under normal conditions of cell proliferation and a loss of viability when the cells are subjected to replication interference[54]. Our Data shows that with decreased Ajuba expression we also have a decrease in proliferation as well as decreased levels of MCM proteins. We therefore investigated if loss of Ajuba leads to an increase of DNA damage. In the pathway enrichment analysis of potential Ajuba binding partners, cell cycle checkpoints, response to DNA damage and Chk1 mediated responses were among the pathways that were found. Additionally, γH2AX as a measure of DNA damage was observed in Ajuba depleted cells indicating that there was an increase in the baseline levels of DNA damage. Moreover, the increased expression of RPA70 which binds to ssDNA and sites of DNA damage binding[48,47,55] gave us a further indication of Ajuba being involved in DNA replication and damage. Supporting our data, Fowler et al. and Kalan et al. described RPA70 as a direct interaction partner of Ajuba and that Ajuba binding to RPA70 inhibits induction of ATR[15,56]. In addition to Ajuba KD cell lines expressing increased levels of γH2AX, they were more sensitive and appeared less able to initiate the DNA repair program in response to irradiation-induce DNA damage. Furthermore, we found Ajuba depleted cells to also express more p-Chk1 which is occurring in presence of DNA damage and leads to cell cycle arrest[57].

In summary, our study provides evidence that Ajuba supports liver cell proliferation associated with development, regeneration, and tumor growth, which may be attributed to its association with DNA replication and repair proteins.

Author's Contributions Conceptualization: N.D., D.S.; Methodology: N.D., J.G, D.S-T., F.A.B, F.B.; Formal Analysis: N.D., D.S.-T.; Data Curation: N.D., D.S.-T., F.A.B, FB, G.L.; Writing-Original Draft Preparation: N.D.; Writing-Review & Editing: N.D. and D.S.; Supervision: D.S.; Funding Acquisition: D.C., D.S. All authors have read and agreed to the published version of the manuscript.

Data Availability Statement

This article is protected by copyright. All rights reserved

Accepted Article

The data that support the findings of this study are available in Tables 1 & 2.

Acknowledgments

We would like to thank Deborah Krauer, Magali Humbert and Prof. Mario Tschan for their help with preparing the lentiviruses; Prof. Charaf Benarafa for his advice designing the generation of the Ajuba KO mice; Dr. Urban Deutsch and Albert Witt for the production of Ajuba KO mice; Prof. Marianna Kruithof-de Julio and Dr. Sofia Karkampouna for their support with the HCC organoids; Prof. Thomas Kaufmann for providing the DEN treated mouse liver samples. We thank the Flow Cytometry & Cell Sorting and Live Cell Imaging core facilities of the Department of Biomedical Research, University of Bern and the Functional Genomics Center Zurich, ETH, University of Zürich for their support with the mass spectrometry. We also thank Isabel Büchi and Dana Leuenberger for technical support; Dr. Adrian Keogh for critically reading the manuscript and the Aclon Foundation for their generous support of the project.

Conflicts of Interest: The authors claim no conflicts of interest

Accepted Article

This article is protected by copyright. All rights reserved

Materials and Methods

Partial hepatectomy model

Mice underwent a standard hepatectomy resecting two thirds of the liver according to previously described protocol[32]. The mice used in this study were 6- to 8-week- (~20 g) female C57BL/6JRccHsd provided by Harlan, the Netherlands. Animals were kept in a temperature-controlled room with a 12-h dark/light cycle. Experiments were done with Institutional Animal Care and Use Committee approval and in strict accord with good animal practice as defined by the Office of Laboratory Animal Welfare. Littermates were randomly assigned to control sham or partial hepatectomy groups. For analgesia, 0.05 mg/kg buprenorphine (Temgesic, Indivior Schweiz AG, Swissmedic Cat. No. 41931) was injected subcutaneously prior to surgery. During surgery, which lasted 20-25 minutes, mice were anesthetized by isoflurane inhalation. The mice were immobilized in a supine position and the liver exposed by transverse laparotomy. Following laparotomy, Vicryl 4.0 suture (Ethicon, VCP496) was used to ligate the left and median liver lobes. The ligated liver lobes were then resected using surgical scissors. The peritoneal cavity was irrigated with saline solution and the abdomen closed using a two-layer running suture. Liver tissue from sham operated mice were used as non-regenerating control. In sham-operated mice, a laparotomy was performed, the liver was manipulated with a cotton-coated stick, irrigated with saline solution, and the abdomen was sutured closed. After PHx livers were allowed to regenerate for various time points up to 7 days. At experimental endpoints, mice were anesthetized by isoflurane inhalation. Blood was collected via the vena cava and centrifuged for serum. Mice were sacrificed by exsanguination. Liver was carefully excised, and tissues were cut in 3 × 3 mm pieces, frozen in liquid nitrogen and stored at −80°C or fixed in 4% formalin overnight at room temperature.

In vivo CCl_4 and DEN liver injury models

C57BL/6 mice were treated for 14 weeks with carbon thetracloride (CCl_4) in order to induce hepatotoxicity and fibrosis development[33,58]. CCl_4 was injected intraperitoneally twice a week using 0.5 ul/g of 20% CCl_4 diluted in olive oil. Control mice were injected with the same volume of olive oil. Diethylnitrosamine (DEN) injection was used to induce an acute phase hepatotoxicity and

This article is protected by copyright. All rights reserved

provoke compensatory regeneration. DEN was injected intraperitoneally at a concentration of (100mg/kg) and liver tissue was harvested 24h post DEN injection.

Cell lines and primary human endothelial and hepatocyte cultures

All human liver cancer cell lines were purchased from American Type Culture Collection (ATCC (Huh7, HepG2, Hep3B, skHep1, C3A, PLC/PRF/5, SNU-387, SNU-423, SNU-449, SNU476. HLE, HLF)) and cultured either in Dulbecco's Modified Eagle's or RPMI medium 1640 (Life Technology) with 10% of FBS, 100 U/mL Penicillin and 100 µg/mL Streptomycin (Life Technology). Note that skHep1 is of endothelial origin as reported by several publications and should be considered with care[59,60,61]. Only Huh7 cell line was cultured in RPMI medium GluatMax with 10% FBS, 100 µg/mL Penicillin/streptomycin (Life Technology). All lines have been tested and are negative for mycoplasma contamination using PCR Mycoplasma Test Kit (Promokine). Primary human endothelial cells (HUVEC) were isolated from umbilical cord and cultured in MCDB 131 medium with 5% of FBS, 10 ng/mL of HEGF (Sigma-Aldrich), 1 ng/mL of hydrocortisone (Sigma-Aldrich) and antibiotics.

Primary human hepatocytes were isolated from consented patients at the University Hospital of Bern undergoing surgical liver resection. Informed consent was obtained prior to surgery in compliance with the local ethics regulations and under approval of local ethics commission. Hepatocytes were cultured according to an established standard procedure[62]and seeded on collagen-coated plastic dishes prior to culture in Dulbecco`s minimum essential medium (DMEM) supplemented with 10% fetal bovine serum, 50 U/mL penicillin, 50 µg/mL streptomycin, and 1 µmol/L dexamethasone. After overnight culture, the medium was replaced by serum-free Williams E medium®glutaMax™.

Monocyte differentiation using PMA

Human monocyte cell line U-937was purchased form American Type Culture Collection (ATCC) and cultured in RPMI-1640 Medium. U-937 differentiation was induced using PMA as previously described in literature[35,36]. U-937 cells were treated for 3 days with PMA, Nocodazole, DMSO or left untreated. PMA (160nM dissolved in DMSO) to induce differentiation into less proliferative Macrophages. Nocodazole treatment (100ng/ml dissolved in DMSO) was used as a positive control

This article is protected by copyright. All rights reserved

for growth arrest and DMSO only as a solvent control. Bright-field microscopy was used to take pictures at day 1 and day 3 after the treatments to show differences in cell number and cell morphology (differentiation status). After 3 days cells were harvested, and RNA extracted using Triazol (Thermo fisher) and further processed for qPCR analysis to detect Ajuba mRNA levels.

Ajuba overexpression using lentiviral transduction

Liver cancer cell line Huh7 was transduced with a lentiviral Ajuba expressing construct as previously described[40]. The Ajuba plasmid was purchased from Harvard PlasmID:Phage_CMV_C_FLAG_HA_IRES_PURO
All experiments were carried out on cells at 25-50% confluence and the efficiency of the transduction was assessed by real-time qRCR and immunoblot.

Cell Proliferation assay (MTT assay)

Cells were seeded in a 96-well plate at a density of 2'000 cells per well in 200 µL of medium. Cells were incubated for 6 hours to adhere to the plate. Every day at the same time, MTT (5mg of thiazolyl blue dissolved in 5 ml DMEM) was added in one tenth of the culture volume (20 µL for 200um plated) in each well (4 wells per time point and condition) and incubated for 1h. Then the medium was discarded and replaced by 200 µL of DMSO. Using the Tecan Infinite 2000, the plate was shaken and read at an absorbance of 570 nm.

HCC patient-derived organoids cultures:

Human HCC tumor tissues were obtained from consented patients at the University Hospital of Bern undergoing surgical liver resection. Informed consent was obtained prior to surgery in compliance with the local ethics regulations and under approval of local ethics commission. HCC tissue as well as adjacent to HCC tissue were used for qPCR analysis. We used resected tissues sampled form HCC patient and sampled resected tissue from outside from the tumor margin as non-malignant control. Tumor tissue was mechanically disrupted and enzymatically digested to obtain 3D organoids culture as previously described[63]. Briefly, tumors were collected in basis medium and mechanically disrupted then dissociated using collagenase type II enzyme mix. Tumor was digested for 1h at 37°C mixing the samples every 20 min. Then the samples were filtered

This article is protected by copyright. All rights reserved

(100um) and erythrocytes lysed using EC lysis buffer. Finally, single cell suspension was achieved using incubation in Accutase™. The single cell suspension was then filtered again (40um) and re-suspended in Matrigel. Drops of Matrigel and single cell suspension were added in a 24-well plate and dried for 30 min at 37°C. Finally, special supplemented medium was added to the Matrigel drops and organoids left several days to from HCC organoids. Human organoids were kept in culture up to several weeks at 37°C in a humidified incubator with 5% of CO2.

Public data acquisition

On the 04.09.2021, HCC RNA-seq expression (counts) and survival data of liver cancer was downloaded from The Cancer Genome Atlas[39].

Survival analysis

The survival curves were calculated with the R function survfit from the R package survival[64] with the formula Surv(time,vitalstatus)~categorie and plotted with the R function ggkm from the R package ggkm[65]. The samples labeled as "primary tumor" were included. The data was separated in high expression (top 20%) and low expression (bottom 80%). Using interactive tools on publicly available data visualization tools such as the Human Protein Atlas the effect of different cutoff threshold can also be tested. 2 samples were discarded due to missing information.

Generation of Ajuba KO mice

Ajuba KO mice were generated using clustered regularly interspaced short palindromic repeats (CRISPR/Cas9) technique and subsequent pronuclear injection. All animal experiments were performed according to the regulations drafted by the Association for Assessment and Accreditation of Laboratory Animal Care. Ajuba KO mice were created in collaboration with the Theodore Kocher institute Bern (TKI). Recombinant Cas9 nuclease, tracrRNA, crRNA and nuclease-free duplex buffer were purchased from IDT. We used two gRNA targeting mouse Ajuba gene creating a 693 kDa deletion in Exon 1. Ajuba mouse protein contains 8 exons and no alternative splice variants. Target sites corresponding to the targeting sgRNA were predicted by the web-based tool (http://crispr.mit.edu). Predicted cleavage sites and considered them as a potential off target event. The specifically designed CRISPR/Cas9 riboprotein complex was microinjected into

This article is protected by copyright. All rights reserved

wild-type zygotes (C57BL/6J) as described by Aida et al.[66]. In short, crRNAs were mixed separately with the tracrRNA and incubated at 95°C for 2 minutes, the tubes were let to cool down at room temperature for at least 15 minutes. Shortly before injection the crRNA-tracrRNA duplexes were mixed with EmbryoMax buffer at room temperature. Finally, the Cas9 protein was added and mixed with the riboprotein complex at 37°C for 20 minutes before being centrifuged at 18'000g for 10minutes at 4°C. The CRISPR/Cas9 riboprotein complex was then microinjected into the male pronucleus of previously fertilized and isolated oocytes. Fertilized oocytes were obtained from superovulating young (4-6 week old). After overnight incubation at 37°C, the oocytes that successfully developed into two cell stage zygotes were transferred into the oviductal ampullae of pseudo-pregnant females using standard protocols (10-15 zygotes per oviduct). We have conducted two separate rounds of pronuclear injections. First round we transferred 90+ 2-cell embryos were transplanted into 6 recipient mice of which 8 pups were born. 5 of these 8 mice survived and were further analyzed. The second series of injections yielded 56 2-cell stage embryos, which were transferred to 4 mice and of which 2 mice survived. The resulting founder mice were genotyped by PCR. Founders were backcrossed with C57BL/6J and mutated alleles in F1 mice were identified by DNA sequencing (Supplementary Figure 5). F1 mice with identical mutations were intercrossed to generate Ajuba KO -/- mice. F2 progeny of 2 distinct Ajuba founder lines were genotyped and used to calculate the generated mendelian ratio of WT, heterozygous and homozygous mice (Supplementary figure 5). All the generated mice were genotyped using ear biopsies and our previously designed primers. Primers were designed using the web tool from National Center for Biotechnology Information (NIH) Primer-BLAST tool for specific primer design[67]. Primer Nr1 was designed to differentiate the genotype of the mice according of the total length of the PCR product. Looking at the total length we could also assess the size of the deletion and using sanger sequencing of the DNA extracted from the PCR products loaded on the agar gel (WT expected size=1400 and KO=700). Analysis of the sequencing was performed using GeneCoder and CodonCode aligner. The sequencing results were used to design specific and unique primers for the different founder lines, targeting the newly created sequence at the deleted regions. Finally, we designed additional WT primers targeting a region found to be deleted in all founder lines, to verify again the presence of the WT band in all the genotyped mice. Alt-R CRISPR-Cas9 TracrRNA; Alt-R S.p Cas9 hifi nuclease 3NLS (in glycerol); Alt-R CRISPR-Cas9

This article is protected by copyright. All rights reserved

crRNA 1 (Cas9.Ajuba.1 sequence: CCCGGACGACACTCGGTTAC /PAM=AGG); Alt-R CRISPR-Cas9 crRNA 2 (Cas9.Ajuba.2 sequence: TGGGCTACGACCAGCGCCAC /PAM=GGG); EmbryoMax buffer (Millipore).

PCR-genotyping protocol:

The biopsies were collected from all mice and lysed using direct PCR (Viagen Biotech) following manufacturers protocol. Shortly, 200ul of lysis buffer mixed with 10% proteinase K (Qiagen) was added to the biopsies and incubated at 55°C on a shaker overnight. The next day, proteinase K is inactivated for 20 min at 95°C. GoTaq 2X PCR master mix (Promega) was used with the genotyping primer pairs. All PCR conditions were as follows: 95°C, 2min; [95°C, 30sec; 58°C, 30sec; 72°C, 45sec] x 32; 72°C, 5min; 4°C forever. PCR products were run on 3% Agarose gels in 1X TAE buffer. After genotyping, the gel bands were cut out and DNA isolated and send for sequencing (Microsynth AG) to determine the exact sequence of the mutation. To assess if the homozygous and heterozygous mice were following the expected mendelian ratios for monohybrid cross 1:2:1 (25% WT, 50% Heterozygous and 25% Homozygous KO), we performed chi-square goodness of fit test. We therefore use the R function chisq.test, comparing the actual and expected nr of genotyped mice.

Lentiviral transduction

Liver cancer cell line Huh7 was transduced with two shRNAs targeting Ajuba and one lentiviral Ajuba expression construct as mentioned above and previously described[40]. The shRNAs were purchased from MISSION™, Sigma-Aldrich. Clone shAjuba1 (coding region) NM-032876.4-1385s1c1. Clone shAjuba2 (non-coding region 2URT) NM_032876.4-2786s1c1
Lentiviral scrambled control shRNA with random sequence Clone shScrambled MISSION® pLKO.1-puro non-mammalian shRNA Control Plasmid. Ajuba expression construct: Clone Ajuba OE Harvard PlasmID:Phage_CMV_C_FLAG_HA_IRES_PURO. All experiments were carried out on cells at 25-50% confluence and the efficiency of the transduction was assessed by real-time qRCR and immunoblot.

This article is protected by copyright. All rights reserved

Western blot

Total protein extraction was performed using RIPA cell lysis buffer (10 mM Tris with pH 8, 1 mM EDTA pH 8, 150 mM NaCl, 0.5% NP40) with addition of protease inhibitors (1mM NaF, 10mM NaVO3, 1mM PMSD, 1X protease inhibitor cocktail - Sigma P1860). The cell lysates were sonicated (Sonopuls, Bandelin), then centrifuged and only the supernatant was kept for further analysis. Snap frozen tissue pieces were dissociated using a TissueLyser (Qiagen) for 2 min at 20 Hz in RIPA buffer. The protein lysate concentrations were determined with the Bio-Rad Protein Assay System (Bio-Rad) as described by the manufacturer. Equal amounts of proteins were separated by SDS–PAGE and transferred onto a nitrocellulose membrane using the iBlot2 Gel transfer device. The membrane then was blocked in 5% non-fat dry milk dissolved in PBS for 1h followed by incubation with the primary antibody overnight at 4°C. After incubation with the HRP conjugated secondary antibody, chemiluminescent reaction was performed with Western Lightning Plus-ECL from Perkin Elmer. Membranes were developed using the x-ray film processor Curix 60 (AGFA). The band size was estimated using Page Ruler™ Prestained Protein Ladder (Fermentas) and Precision Plus Protein™ DUAL Color Standards (BIO-RAD, #161-0374). Primary antibodies used were rabbit monoclonal anti-Ajuba (1:1000 dilution, Cell Signalling), yH2Ax (1:1000 dilution,P-Histone H2AX (Ser139), Millipore), RPA70 (1:1000 dilution, Cell signaling). HRP-conjugated secondary antibodies used were goat anti-rabbit (Dako). β-actin-HRP (1:100'000 dilution, Sigma) as well as antibody against TATA-Box Binding Protein (anti-TBP) (1:1000 dilution, Cell Signaling) were used as a loading control.

Quantitative real-time reverse transcription PCR

Total RNA was isolated from human samples and cell lines using Triazole (Thermo fisher) according to manufacturer's protocol. The quality and concentration of RNA were measured using Nanodrop 2000 Spectrophotometer (Thermo Scientific). 500 ng of total RNA was used for cDNA synthesis using Omniscript RT Kit 200 (Qiagen). mRNA was analysed by quantitative RT–PCR with TaqMan gene expression assays and reagents according to the standard protocols (Applied Biosystem), using specific primers and housekeeping genes 18S FAM as control. We used the TaqMAN ViiA TM 7 Real-time PCR system from Applied BioSystems for the amplification steps and data collection. Log 2-fold changes were computed using the $^{\Delta\Delta}Ct$ method. Ct values of target genes (TG) were

This article is protected by copyright. All rights reserved

calculated relative to a reference gene (RG, 18S) using the following formula: $\Delta Ct_{TG} = Ct_{TG} - Ct_{RG}$. Experimental groups (TG) are normalized to control group (CG): $^{\Delta\Delta}Ct = {}^{\Delta}Ct_{TG} - {}^{\Delta}Ct_{CG}$, and fold increase = $^{2-\Delta\Delta}Ct$.

Colony formation assay

Colony formation assay was performed as previously described[68]. Briefly, 1'000 cells per well were platted in triplicates into 6-well plates and incubated for 7 days. To stop the colony formation, the medium was removed, and cells were washed twice with DPBS before being dried. Crystal violet was used to stain the cells (3 g crystal violet, 99.9 mL methanol, 49.9 mL acetic acid) by incubating each well for 30 min at room temperature. The number of colonies were counted using the Colcount (Oxford Optromix, Abingdon, UK).

In vivo syngeneic tumor model

RIL-175 cells, were previously transfected with lentivirus to KD Ajuba, and shScrambled control were used to inject subcutaneously on the flank of C57BL/6J mice. Protocol was adapted from Brown et al.[69] in short, $1x10^6$ cells were injected N=5 mice per condition were used and tumor was measured ever second day using a digital caliper under isoflurane. Tumor volume was calculated according to the modified ellipsoid formula volume = $(4/3)\times\pi\times(length/2)\times(width/2)\times(height/2)$[70]. Mice were harvested two weeks after injection and tumors carefully excised and SNAP frozen or paraformaldehyde preserved for further analysis.

Angiogenesis tube formation assay in 3D Matrigel:

Primary endothelial cells were isolated from the umbilical cord to generate HUVEC. Ajuba was KD using shRNA and then a vascular tube formation assay was performed as previously described[70]. Briefly, 150'000 HUVEC were plated per well in a 96-well plate, that was coated with 30 µL of Matrigel® (BD Biosciences). Pictures were taken with a Leica camera and afterwards analyzed by a semi-automated plug-in for ImageJ software as previously described[41]. All experiments were performed in triplicate.

This article is protected by copyright. All rights reserved

Immunofluorescence

Tissue samples were fixed in 4% formaldehyde for 24h then processed and embedded in paraffin. Paraffin blocks were sectioned with Leica Microtome in 6um thick slides. Sections were stained using Ajuba antibody (Novus biologicals, NBP1-39570, concentration 1:50) overnight at 4°C. The secondary antibody, anti-rabbit Cy3 (life technologies, concentration 1:300), was incubated for 2 hours in antibody diluent (Dako antibody diluents with Background reducing components). Coverslips were mounted with VECTASHIELD Antifade Mounting Medium with DAPI (Vector Laboratories, H-1500) and fluorescence images were taken using an automated inverted microscope (Leica DMI4000 B).

Flow-cytometry assessment of S-phase entry

Huh7 cell lines with Ajuba KD and OE were synchronized at the G1/S transition of cell cycle using thymidine, an inhibitor of DNA synthesis. EdU integration was used to assess the percentage of cells in S-phase at different time points, over the time course of 24h. Cell synchronization protocol was adapted and optimized for Huh7 from Macheret et al[43]. Cells were treated with 2mM of thymidine for 18 h to synchronize cells at early S-phase of cell cycle (G1/S boundary). After thymidine synchronization the cells were trypsinized and washed twice in warm medium then released in warm media containing 25 µM EdU for various time points (Invitrogen, Cat. No. A10044). Cells were collected every two hours and fixed with 90% methanol overnight as previously described[44]. The cells were prepared for flow cytometry using the Click-it Kit (Invitrogen Cat. No. C-10420) according to the manufacturer's instructions. The genomic DNA was stained with propidium iodide (Sigma, Cat. No. 81845) in combination with RNAse (Roche, Cat. No. 11119915001). EdU-DNA content profiles were then acquired by flow cytometry (SORP LSR II) to assess the percentage of cells that entered S-phase in each condition at each time point.

RT2 Microarray and data analysis

Cell cycle RT2 profiler PCR gene arrays were purchased form Qiagen. Total RNA was isolated form human HCC cell line Huh7 were we previously KD and OE Ajuba protein using Promega extraction kit according to manufacturer's instruction. The quality and concentration of the RNA were measured with the Agilent 2100 BioAnalyzer. High quality RNA samples (RIN> 9) were then reverse

This article is protected by copyright. All rights reserved

transcribed using the First strand synthesis kit form Qiagen. The samples were prepared in duplicates in order to have enough cDNA for the two different array plates. Samples were then loaded to the cell cycle array plate according to Manufacturer's instructions. Finally, the data was analyses using the GeneGlobe online web analysis tool provided by Qiagen. After selecting the correct RT2 profiler and the species used in the experiment, the Raw data was uploaded into the dataset via a previously prepared excel sheet of all the qPCR plates. Using the sample Manager, Control group was defined as the scrambled cell line whereas the other samples were named Group 1-5. Sample Ct- Cut-off was set to 35 for both the arrays. A quality control was performed by the program to check for PCR array reproducibility, reverse transcription control and Genomic DNA contamination. Data was normalized to an average of 4 selected housekeeping genes. For the cell cycle array plate housekeeping genes: B2M, GAPDH, HPRT1 and RPLPO were used, and for the hippo pathway array plate ACTB B2M, GAPDH and RPLP0 were used. Comparative heat maps and fold change was calculated by determining the ratio of mRNA levels to control values using the ΔCt method ($2^{-\Delta\Delta Ct}$). Data was depicted with a heatmap using R.

Immunoprecipitation and subsequent Mass spectrometry (MS)

Immunoprecipitation was performed using the Pierce MS-compatible magnetic IP kit (streptavidin) from thermos scientific. Huh7 cell lines, Ajuba OE containing an HA-tag and shScrambled containing no HA-tag were used respectively as a sample and as a control for the experiments. Protein was isolated according to manufactures instruction 48h after plating with the slight modification of adding Proteinase inhibitors and PMSF to the cell lysis buffer. The protein concentration was measured using Bradford assay, and IP was performed with 1000ng of protein and 60 µl of biotinylated anti-HA Antibody (100ug/ml). The cell lysate was incubated over night with the specific biotinylated ab at 4°C. The next day, antigen /ab complex to streptavidin magnetic beads was incubated for 2h at 4°C and then for 20 min at RT. The samples were run in duplicated and sent to the Functional Genomics Center Zurich, ETH, University of Zurich where samples were further processed and analyzed for LC/MS/MS.

Immunoprecipitation analysis

This article is protected by copyright. All rights reserved

Immunoprecipitation was analyzed using scaffold4. Protein threshold was set to 1.0% FDR and min number of peptides to 2. Peptide threshold 0.1% FDR. Database searches were performed by using the Mascot (Swiss_Prot, human) search program which identified a total of 1072 proteins. We filtered out the proteins that were uniquely expressed in Ajuba OE and named them Class I. From the proteins that were detected in both samples we then filtered out the ones that had a 2-fold higher expression of total unique peptide count in OE compared to its control and named them Class II. Resulting in a total of 247 proteins. All other proteins were not used for further analysis. The full mass spectrometry report table displaying all the detected proteins is available in Table 1 and the list for all proteins of Class I and Class II is available in Table 2.

Immunoprecipitation and Western blot analysis

Immunoprecipitation was carried out overnight at 4°C on 800µg of total HuH7 Ajuba OE and HuH7 parental cells lysate with Protein A or G agarose/Sepharose beads (Abcam, ab193262) and 5 µg/ml of monoclonal anti-HA-Biotin (Roche, 12158167001). Beads were washed four times with PBS/Tween 0.1% to remove unbound proteins. Interacting proteins were detected by Western blot using the following antibodies: RPA70 (1:1000, Cell Signaling #2198), MCM2 (Cell Signaling #3619), MCM3 (1:1000, Cell Signaling #4003), MCM7 (1:1000, Cell Signaling #3735), SKP2 (1:1000, Cell Signaling #2652), CHK1 (1:1000, Cell Signaling #2360).

Venn Diagram

Venn diagrams were drawn using custom Venn diagrams from Bioinformatics & Evolutionary Genomics web tools[71].

String Visualization

Protein selected (Class I and Class II) from the MS analysis were plotted on string-db.org in order to visualize known interactions with Ajuba protein[41].

Pathway Enrichment Analysis

Pathway enrichment analysis was performed using Metascape Gene Annotation & Analysis Resource[72]. We used the proteins selected from the MS analysis of Class I, Class II and the

This article is protected by copyright. All rights reserved

combination of Class I and II to display pathway enrichment. The top 20 statistically significant families of pathways are displayed.

Immunocytochemistry

HCC cell lines were grown on glass cover slips in 8-plates (50'000 cells per well). Cells were fixed with 4% formaldehyde, permeabilized and blocked in 5% goat serum (DAKO, X0907), 0.3% Triton-X-100 (Sigma-Aldrich) in DPBS and stained with anti- γH2AX (γH2Ax (1:500 Millipore, P-Histone H2AX (Ser139) and matched with Alexa Fluor® (AF) 647 conjugated secondary antibodies (Life Technologies 1:1000). Nuclei were counterstained with DAPI (1:5000), coverslips were mounted with Vectashield Antifade Mounting Medium (Vector Laboratories, H-1000) and fluorescence images were taken using the Panoramic 250 Flash II slide scanner (3DHistech).

FACS assessment of DNA damage and DNA damage repair:

To assess the DNA damage in Huh7 cell lines where Ajuba was previously KD and OE, we used the FlowCellect™ Histone H2A.X Phosphorylation Assay Kit according to the manufacturer's instructions. To assess the DNA damage repair capacity of the different cell lines, we irradiated the cells with 2 Gray using Gammcell 40 (Best Theratronics) and used γH2AX as a readout as previously described[74]. The FACS readout was then performed using the H2A.X Phosphorylation Assay Kit 2h and 4h after a 2 Gray irradiation.

Sensitivity to Irradiation

In 6-well plates, cells were platted with a density of 1'000 cells in 200 µl medium per well. After letting the cells adhere for 6h, the plates underwent irradiation in a Gammacell 40 (Best Theratronics) at the following doses: 0, 2, 3, 4, 5, 6 and 8 Gray as previously described[40]. Non-irradiated cells were used as a control. The sensitivity after irradiation was assessed by the cells capacity to form colonies as described under Colony formation assay.

Graphs and Statistical analysis

R was used for the computation of publicly available RNA-seq data and RT2 microarray experiments, graphs were displayed using R-package ggplot2[73]. Scaffold4 was used for the analysis of the mass spectrometry data. The graphs and the statistics for the remaining graphs were done

This article is protected by copyright. All rights reserved

by using GraphPad Prism software. *P*-values were calculated as mentioned on the figure legend using either. an unpaired, two-tailed Student's *t*-test, two-way ANOVA with no repeated measures and Tukey adjusted for multiple comparison, one-way ANOVA with correction for multiple comparison using Dunnet test or log-rank test. For all analyses NS denotes $p>0.05$, * $p<0.05$, ** $p<0.01$, *** $p<0.001$, **** $p<0.0001$.

Accepted Article

This article is protected by copyright. All rights reserved

Accepted Article

References

1 Michalopoulos, G. K. & DeFrances, M. C. Liver regeneration. *Science* **276**, 60-66, doi:10.1126/science.276.5309.60 (1997).

2 Malumbres, M. & Barbacid, M. To cycle or not to cycle: a critical decision in cancer. *Nat Rev Cancer* **1**, 222-231, doi:10.1038/35106065 (2001).

3 Branzei, D. & Foiani, M. Maintaining genome stability at the replication fork. *Nat Rev Mol Cell Biol* **11**, 208-219, doi:10.1038/nrm2852 (2010).

4 Fragkos, M., Ganier, O., Coulombe, P. & Méchali, M. DNA replication origin activation in space and time. *Nat Rev Mol Cell Biol* **16**, 360-374, doi:10.1038/nrm4002 (2015).

5 Moiseeva, T. *et al.* ATR kinase inhibition induces unscheduled origin firing through a Cdc7-dependent association between GINS and And-1. *Nat Commun* **8**, 1392, doi:10.1038/s41467-017-01401-x (2017).

6 Zhang, C. *et al.* Super-enhancer-driven AJUBA is activated by TCF4 and involved in epithelial-mesenchymal transition in the progression of Hepatocellular Carcinoma. *Theranostics* **10**, 9066-9082, doi:10.7150/thno.45349 (2020).

7 Goyal, R. K. *et al.* Ajuba, a novel LIM protein, interacts with Grb2, augments mitogen-activated protein kinase activity in fibroblasts, and promotes meiotic maturation of Xenopus oocytes in a Grb2- and Ras-dependent manner. *Mol Cell Biol* **19**, 4379-4389, doi:10.1128/mcb.19.6.4379 (1999).

8 Srichai, M. B. *et al.* A WT1 co-regulator controls podocyte phenotype by shuttling between adhesion structures and nucleus. *J Biol Chem* **279**, 14398-14408, doi:10.1074/jbc.M314155200 (2004).

9 Sharp, T. V. *et al.* LIM domains-containing protein 1 (LIMD1), a tumor suppressor encoded at chromosome 3p21.3, binds pRB and represses E2F-driven transcription. *Proc Natl Acad Sci U S A* **101**, 16531-16536, doi:10.1073/pnas.0407123101 (2004).

10 Jia, H., Peng, H. & Hou, Z. Ajuba: An emerging signal transducer in oncogenesis. *Pharmacol Res* **151**, 104546, doi:10.1016/j.phrs.2019.104546 (2020).

11 Alégot, H. *et al.* Recruitment of Jub by α-catenin promotes Yki activity and. *J Cell Sci* **132**, doi:10.1242/jcs.222018 (2019).

12 Marie, H. *et al.* The LIM protein Ajuba is recruited to cadherin-dependent cell junctions through an association with alpha-catenin. *J Biol Chem* **278**, 1220-1228, doi:10.1074/jbc.M205391200 (2003).

13 Chen, X., Stauffer, S., Chen, Y. & Dong, J. Ajuba Phosphorylation by CDK1 Promotes Cell Proliferation and Tumorigenesis. *J Biol Chem* **291**, 14761-14772, doi:10.1074/jbc.M116.722751 (2016).

This article is protected by copyright. All rights reserved

14 Haraguchi, K. *et al.* Ajuba negatively regulates the Wnt signaling pathway by promoting GSK-3beta-mediated phosphorylation of beta-catenin. *Oncogene* **27**, 274-284, doi:10.1038/sj.onc.1210644 (2008).

15 Fowler, S., Maguin, P., Kalan, S. & Loayza, D. LIM Protein Ajuba associates with the RPA complex through direct cell cycle-dependent interaction with the RPA70 subunit. *Sci Rep* **8**, 9536, doi:10.1038/s41598-018-27919-8 (2018).

16 Gao, Y. B. *et al.* Genetic landscape of esophageal squamous cell carcinoma. *Nat Genet* **46**, 1097-1102, doi:10.1038/ng.3076 (2014).

17 Zhang, L. *et al.* Genomic analyses reveal mutational signatures and frequently altered genes in esophageal squamous cell carcinoma. *Am J Hum Genet* **96**, 597-611, doi:10.1016/j.ajhg.2015.02.017 (2015).

18 Pickering, C. R. *et al.* Mutational landscape of aggressive cutaneous squamous cell carcinoma. *Clin Cancer Res* **20**, 6582-6592, doi:10.1158/1078-0432.CCR-14-1768 (2014).

19 Shi, X. *et al.* AJUBA promotes the migration and invasion of esophageal squamous cell carcinoma cells through upregulation of MMP10 and MMP13 expression. *Oncotarget* **7**, 36407-36418, doi:10.18632/oncotarget.9239 (2016).

20 Song, K. *et al.* Identification of genes with universally upregulated or downregulated expressions in colorectal cancer. *J Gastroenterol Hepatol* **34**, 880-889, doi:10.1111/jgh.14529 (2019).

21 Bi, L. *et al.* AJUBA increases the cisplatin resistance through hippo pathway in cervical cancer. *Gene* **644**, 148-154, doi:10.1016/j.gene.2017.11.017 (2018).

22 Liang, X. H. *et al.* LIM protein JUB promotes epithelial-mesenchymal transition in colorectal cancer. *Cancer Sci* **105**, 660-666, doi:10.1111/cas.12404 (2014).

23 Jia, H. *et al.* The LIM protein AJUBA promotes colorectal cancer cell survival through suppression of JAK1/STAT1/IFIT2 network. *Oncogene* **36**, 2655-2666, doi:10.1038/onc.2016.418 (2017).

24 Yang, D. *et al.* Smad1 promotes colorectal cancer cell migration through Ajuba transactivation. *Oncotarget* **8**, 110415-110425, doi:10.18632/oncotarget.22780 (2017).

25 Zhang, M. *et al.* Mutations of the LIM protein AJUBA mediate sensitivity of head and neck squamous cell carcinoma to treatment with cell-cycle inhibitors. *Cancer Lett* **392**, 71-82, doi:10.1016/j.canlet.2017.01.024 (2017).

26 Zhang, B. *et al.* The LIM protein Ajuba/SP1 complex forms a feed forward loop to induce SP1 target genes and promote pancreatic cancer cell proliferation. *J Exp Clin Cancer Res* **38**, 205, doi:10.1186/s13046-019-1203-2 (2019).

Accepted Article

This article is protected by copyright. All rights reserved

Accepted Article

27 Tanaka, I. *et al.* LIM-domain protein AJUBA suppresses malignant mesothelioma cell proliferation via Hippo signaling cascade. *Oncogene* **34**, 73-83, doi:10.1038/onc.2013.528 (2015).

28 Liu, M. *et al.* Ajuba inhibits hepatocellular carcinoma cell growth via targeting of β-catenin and YAP signaling and is regulated by E3 ligase Hakai through neddylation. *J Exp Clin Cancer Res* **37**, 165, doi:10.1186/s13046-018-0806-3 (2018).

29 Jia, L. *et al.* Androgen receptor-regulated miRNA-193a-3p targets AJUBA to promote prostate cancer cell migration. *Prostate* **77**, 1000-1011, doi:10.1002/pros.23356 (2017).

30 Du, P. *et al.* Comprehensive genomic analysis of Oesophageal Squamous Cell Carcinoma reveals clinical relevance. *Sci Rep* **7**, 15324, doi:10.1038/s41598-017-14909-5 (2017).

31 Le, Y. *et al.* Knockout of Ajuba Attenuates the Growth and Migration of Hepatocellular Carcinoma Cells. *Cytogenet Genome Res* **160**, 650-658, doi:10.1159/000512264 (2020).

32 Loforese, G. *et al.* Impaired liver regeneration in aged mice can be rescued by silencing Hippo core kinases MST1 and MST2. *EMBO Mol Med* **9**, 46-60, doi:10.15252/emmm.201506089 (2017).

33 Tolba, R., Kraus, T., Liedtke, C., Schwarz, M. & Weiskirchen, R. Diethylnitrosamine (DEN)-induced carcinogenic liver injury in mice. *Lab Anim* **49**, 59-69, doi:10.1177/0023677215570086 (2015).

34 Scholten, D., Trebicka, J., Liedtke, C. & Weiskirchen, R. The carbon tetrachloride model in mice. *Lab Anim* **49**, 4-11, doi:10.1177/0023677215571192 (2015).

35 Wu, J. *et al.* [The role of TNF-alpha in the growth and differentiation of U937 cells induced by PMA and IFN-gamma]. *Shi Yan Sheng Wu Xue Bao* **27**, 307-313 (1994).

36 Song, M. G. *et al.* NRF2 Signaling Negatively Regulates Phorbol-12-Myristate-13-Acetate (PMA)-Induced Differentiation of Human Monocytic U937 Cells into Pro-Inflammatory Macrophages. *PLoS One* **10**, e0134235, doi:10.1371/journal.pone.0134235 (2015).

37 Kallas, A., Pook, M., Maimets, M., Zimmermann, K. & Maimets, T. Nocodazole treatment decreases expression of pluripotency markers Nanog and Oct4 in human embryonic stem cells. *PLoS One* **6**, e19114, doi:10.1371/journal.pone.0019114 (2011).

38 Flomerfelt, F. A. & Gress, R. E. Analysis of Cell Proliferation and Homeostasis Using EdU Labeling. *Methods Mol Biol* **1323**, 211-220, doi:10.1007/978-1-4939-2809-5_18 (2016).

39 Weinstein, J. N. *et al.* The Cancer Genome Atlas Pan-Cancer analysis project. *Nat Genet* **45**, 1113-1120, doi:10.1038/ng.2764 (2013).

40 Dommann, N. *et al.* The LIM Protein Ajuba Augments Tumor Metastasis in Colon Cancer. *Cancers (Basel)* **12**, doi:10.3390/cancers12071913 (2020).

This article is protected by copyright. All rights reserved

41 **Carpentier G** in *Angiogenesis Analyzer for ImageJ. 4th ImageJ User and Developer Conference proceedings* (eds Martinelli M, Courty J, & Cascone I.) (Mondorf-les-Bains, Luxembourg. ISBN: 2-919941-18-6 : 198-201, 2012., 2012).

42 Chen, G. & Deng, X. Cell Synchronization by Double Thymidine Block. *Bio Protoc* **8**, doi:10.21769/BioProtoc.2994 (2018).

43 Macheret, M. *et al.* High-resolution mapping of mitotic DNA synthesis regions and common fragile sites in the human genome through direct sequencing. *Cell Res* **30**, 997-1008, doi:10.1038/s41422-020-0358-x (2020).

44 Macheret, M. & Halazonetis, T. D. Intragenic origins due to short G1 phases underlie oncogene-induced DNA replication stress. *Nature* **555**, 112-116, doi:10.1038/nature25507 (2018).

45 Stark, C. *et al.* BioGRID: a general repository for interaction datasets. *Nucleic Acids Res* **34**, D535-539, doi:10.1093/nar/gkj109 (2006).

46 Das Thakur, M. *et al.* Ajuba LIM proteins are negative regulators of the Hippo signaling pathway. *Curr Biol* **20**, 657-662, doi:10.1016/j.cub.2010.02.035 (2010).

47 Liu, V. F. & Weaver, D. T. The ionizing radiation-induced replication protein A phosphorylation response differs between ataxia telangiectasia and normal human cells. *Mol Cell Biol* **13**, 7222-7231, doi:10.1128/mcb.13.12.7222 (1993).

48 Zou, Y., Liu, Y., Wu, X. & Shell, S. M. Functions of human replication protein A (RPA): from DNA replication to DNA damage and stress responses. *J Cell Physiol* **208**, 267-273, doi:10.1002/jcp.20622 (2006).

49 Loganathan, S. K. *et al.* Rare driver mutations in head and neck squamous cell carcinomas converge on NOTCH signaling. *Science* **367**, 1264-1269, doi:10.1126/science.aax0902 (2020).

50 Fagerberg, L. *et al.* Analysis of the human tissue-specific expression by genome-wide integration of transcriptomics and antibody-based proteomics. *Mol Cell Proteomics* **13**, 397-406, doi:10.1074/mcp.M113.035600 (2014).

51 Schleicher, K. & Schramek, D. AJUBA: a regulator of epidermal homeostasis and cancer. *Exp Dermatol*, doi:10.1111/exd.14272 (2020).

52 Pratt, S. J. *et al.* The LIM protein Ajuba influences p130Cas localization and Rac1 activity during cell migration. *J Cell Biol* **168**, 813-824, doi:10.1083/jcb.200406083 (2005).

53 Kanungo, J., Pratt, S. J., Marie, H. & Longmore, G. D. Ajuba, a cytosolic LIM protein, shuttles into the nucleus and affects embryonal cell proliferation and fate decisions. *Mol Biol Cell* **11**, 3299-3313 (2000).

Accepted Article

This article is protected by copyright. All rights reserved

Accepted Article

54 Crevel, I. *et al.* Decreased MCM2-6 in Drosophila S2 cells does not generate significant DNA damage or cause a marked increase in sensitivity to replication interference. *PLoS One* **6**, e27101, doi:10.1371/journal.pone.0027101 (2011).

55 Zhou, B. B. & Elledge, S. J. The DNA damage response: putting checkpoints in perspective. *Nature* **408**, 433-439, doi:10.1038/35044005 (2000).

56 Kalan, S., Matveyenko, A. & Loayza, D. LIM Protein Ajuba Participates in the Repression of the ATR-Mediated DNA Damage Response. *Front Genet* **4**, 95, doi:10.3389/fgene.2013.00095 (2013).

57 Enders, G. H. Expanded roles for Chk1 in genome maintenance. *J Biol Chem* **283**, 17749-17752, doi:10.1074/jbc.R800021200 (2008).

58 Dong, S. *et al.* Mechanisms of CCl4-induced liver fibrosis with combined transcriptomic and proteomic analysis. *J Toxicol Sci* **41**, 561-572, doi:10.2131/jts.41.561 (2016).

59 Heffelfinger, S. C., Hawkins, H. H., Barrish, J., Taylor, L. & Darlington, G. J. SK HEP-1: a human cell line of endothelial origin. *In Vitro Cell Dev Biol* **28A**, 136-142, doi:10.1007/BF02631017 (1992).

60 Boyault, S. *et al.* Transcriptome classification of HCC is related to gene alterations and to new therapeutic targets. *Hepatology* **45**, 42-52, doi:10.1002/hep.21467 (2007).

61 Rebouissou, S., Zucman-Rossi, J., Moreau, R., Qiu, Z. & Hui, L. Note of caution: Contaminations of hepatocellular cell lines. *J Hepatol* **67**, 896-897, doi:10.1016/j.jhep.2017.08.002 (2017).

62 Portmann, S. *et al.* Antitumor effect of SIRT1 inhibition in human HCC tumor models in vitro and in vivo. *Mol Cancer Ther* **12**, 499-508, doi:10.1158/1535-7163.MCT-12-0700 (2013).

63 Karkampouna, S. *et al.* CRIPTO promotes an aggressive tumour phenotype and resistance to treatment in hepatocellular carcinoma. *J Pathol* **245**, 297-310, doi:10.1002/path.5083 (2018).

64 Therneau, T. M. Vol. . *ISBN0-387-98784-3* (ed *Patricia M. Grambsch*) (Springer, New York, 2000).

65 Way, M. (https://rdrr.io/github/michaelway/ggkm/, R package version 1.0, 2016).

66 Aida, T. *et al.* Cloning-free CRISPR/Cas system facilitates functional cassette knock-in in mice. *Genome Biol* **16**, 87, doi:10.1186/s13059-015-0653-x (2015).

67 National Library of Medicine. *Tool for finding specific primers National Center for Biotechnology Information*.

68 Franken, N. A., Rodermond, H. M., Stap, J., Haveman, J. & van Bree, C. Clonogenic assay of cells in vitro. *Nat Protoc* **1**, 2315-2319, doi:10.1038/nprot.2006.339 (2006).

69 Brown, Z. J. *et al.* Indoleamine 2,3-dioxygenase provides adaptive resistance to immune checkpoint inhibitors in hepatocellular carcinoma. *Cancer Immunol Immunother* **67**, 1305-1315, doi:10.1007/s00262-018-2190-4 (2018).

This article is protected by copyright. All rights reserved

70 Gavini, J. *et al.* Verteporfin-induced lysosomal compartment dysregulation potentiates the effect of sorafenib in hepatocellular carcinoma. *Cell Death Dis* **10**, 749, doi:10.1038/s41419-019-1989-z (2019).

71 Peer, V. d. *Venn diagrams for Bioinformatics & Evolutionary Genomics Web tool Diagrams CadcV. http://bioinformatics.psb.ugent.be/webtools/Venn/*.

72 Zhou, Y. *et al.* Metascape provides a biologist-oriented resource for the analysis of systems-level datasets. *Nat Commun* **10**, 1523, doi:10.1038/s41467-019-09234-6 (2019).

73 Wickham H. ggplot2: Elegant graphics for data Analysis (Springer Verlag New York, 2016).

74 Mariotti, L. G. *et al.* Use of the γ-H2AX assay to investigate DNA repair dynamics following multiple radiation exposures. *PLoS One* **8**, e79541, doi:10.1371/journal.pone.0079541 (2013).

Accepted Article

This article is protected by copyright. All rights reserved

Figure legends

Figure 1 Ajuba expression coincides with cell proliferation in normal and liver malignant cells.
(A) Ajuba mRNA expression level in liver tissue pre- and at different time points post 70% PHx, statistical test used: one-way ANOVA with Dunnett's multiple comparison test, error bars show SD, n=3. (B) Ajuba mRNA expression level measured by RT-qPCR in mouse livers after either 14-week treatment with CCl_4 (0.5 ul/g of 20% CCl_4) or 24h after DEN injection (100mg/kg), olive oil was used as a vehicle, statistical test used: unpaired t-test, error bars show SD, n=3. (C) Ajuba mRNA expression level measured by RT-qPCR liver cancer cell lines and normalized to isolated human hepatocytes, statistical test used: t-test with multiple comparison correction Holm-Sidak, error bars show SD, n=3. (D) MTT proliferation assay comparing Parental, shScrambled and Ajuba OE cell lines. The absorbance was measured at 570 nm one hour after MTT addition over the span of 5 days. Statistical test used: two-way ANOVA with Tukey's multiple comparison test, error bars show SD, n=2 one representative plot is shown with technical quadruplicates (E) Ajuba mRNA expression in primary human hepatocytes, human liver tissue isolated from HCC or form tissue adjacent to the HCC tumor tissue and HCC derived human organoids. Statistical test used: unpaired t-test, error bars show SD, n=3/control and n=4/group. (F) 10-year Kaplan Meyer survival curves were generated with data from TCGA and used to calculate HCC patient survival according to their Ajuba expression (high=top 20%, n=73) and low expression (low=bottom 80%, n=296), statistics was computed using log-rank test, p-value = 0.0125. For all analyses ns denotes $p > 0.05$, * $p < 0.05$, ** $p < 0.01$, *** $p < 0.001$, **** $p < 0.0001$.

Figure 2. Decreased Ajuba expression leads to decreased cell proliferation.
(A) Percentage of Ajuba -/-, Ajuba +/- and WT mice after genotyping F2 generation of Ajuba KO founder lines 1&2 mice (N=400, generated by CRISPR/Cas9 technology). Expected Mendelian ratios for monohybrid cross 1:2:1 (25% WT, 50% Heterozygous and 25% Homozygous KO) are depicted as a reference in a dashed line, Chi-squared goodness of fit test was performed comparing found genotypes with expected mendelian rations, p-value < 2.2e-16. (B) Ajuba protein expression in Huh7 cell line with Ajuba KD. (C) Proliferation assay measuring the absorbance at 570 nm 1 hour after addition of MTT over the span of 5 days. Statistical test used: two-way ANOVA with Tukey's multiple comparison test, error bars show SD, n=3 one representative plot is

This article is protected by copyright. All rights reserved

shown with technical triplicates. (D) Colony formation assay in Huh7 cell lines in a 6-well plate and letting the cells proliferate for 7 days as well as the representative picture of the 6-well plate after crystal violet staining, statistical test used: unpaired t-test, error bars show SD, in triplicates. (E) Graph displaying the area under the curve form the tumor volumes of a subcutaneous syngeneic tumors (RIL-175 cell) in BL/6 WT mice, statistical test used: unpaired t-test, error bars show SD, n=5. (F) Vascular tube formation assay in primary endothelial HUVEC and a representative bright field pictures (5x), statistical test used: unpaired t-test, error bars show SD, in triplicates. For all analyses ns denotes $p > 0.05$, * $p < 0.05$, ** $p < 0.01$, *** $p < 0.001$, **** $p < 0.0001$.

Figure 3. 3 Ajuba has a nuclear localization in proliferation cells and involved in DNA replication

(A) Liver sections from control, HCC tissue and a regenerating liver 72h post PHx stained for Ajuba and Dapi. White bar represents 100µm. (Images taken with a Leica DMI 4000 B microscope). (B) DNA replication dynamics studied in Huh7 cell lines with Ajuba KD and OE. The percentage of EdU positive cells were assessed over the timespan of 24h after release from thymidine synchronization. EdU incorporation was detected using FACS analysis with click it staining and total DNA content was measured with propidium iodide (PI). P-values were computed using two-way ANOVA with no repeated measures and Tukey's multiple comparison correction. (D) Cell cycle related gene expression in Ajuba shscrambled and depleted cell lines using RT^2 qPCR profiler array plate from Qiagen. For all analyses ns denotes $p > 0.05$, * $p < 0.05$, ** $p < 0.01$, *** $p < 0.001$, **** $p < 0.0001$.

Figure 4 Ajuba is associated with DNA replication genes.

(A) Ajuba protein expression of Ajuba OE Huh7 cell line using lentiviral transduction. (B) Venn diagram displaying the total number of proteins identified in MS (settings used: prot 1.0% FDR, 2 peptides, pept 0.1% FDR) and showing the selection criteria for further analysis of Class I and Class II proteins (>log 2-fold change) Huh7 cell lines with Ajuba OE containing an HA-tag and control cell line a scrambled control without HA-tag were used. (C) Volcano plot of all proteins detected. (D) Pathway enrichment analysis of binding partners (Class I and II) of Ajuba using Metascape found after immunoprecipitation of Ajuba OE cells using HA-tag. (E) Immunoprecipitation and western blot analysis of Huh77 Ajuba OE and parental cell lysate. Protein A or G agarose/Sepharose beads were used as control. Cell lysates were incubated over night with anti-HA-Biotin ab.

This article is protected by copyright. All rights reserved

Figure 5 Ajuba depletion leads to increased DNA damage expression.

(A) Immunofluorescent pictures of Huh7 cell lines staining for yH2Ax. White bar represents 100µm (B) Percentage of yH2Ax positive cells assessed using FACS analysis and a DNA damage staining kit (FlowCellect™), statistical test used: unpaired t-test, error bars show SD, n=4. (C) Protein expression of yH2Ax assessed by western blot in Huh7 cell lines with Ajuba KD. β-actin was used as a loading control. (D) Western blot analysis of Huh7 cell lines with Ajuba KD stained for RPA70 and p-Chk1. β-actin was used as a loading control. (E) Percentage of colonies that survived after a 3 gray irradiation in Huh7 cell lines, statistical test used: unpaired t-test, error bars show SD, in triplicates. The colonies were stained with crystal violet and counted with ColCounter. Statistics was computed with Graphpad using non-irradiated cells as a measure of 100% (F) Percentage of DNA damage repair that occured between 2 and 4h after a 2 Gray irradiation. FACS analysis was used to compute the percentage of yH2Ax posistve cells 2 and 4h. To compute the percentage of repair 2h time point was considered as 100% damage, statistical test used: unpaired t-test, error bars show SD, n=2. For all analyses ns denotes $p > 0.05$, * $p < 0.05$, ** $p < 0.01$, *** $p < 0.001$, **** $p < 0.0001$.

Accepted Article

This article is protected by copyright. All rights reserved

Figure 1

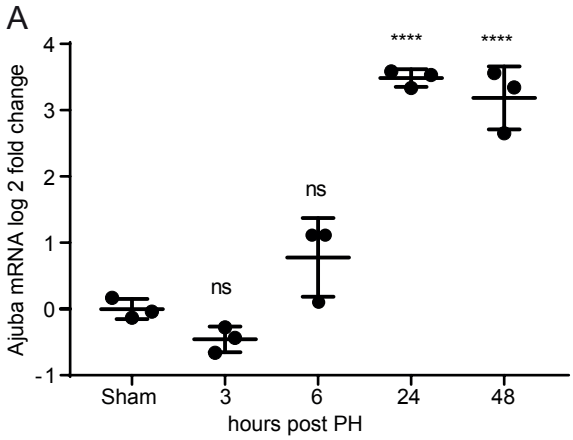
A
Ajuba mRNA log 2 fold change
hours post PH
Sham
3
6
24
48
ns
ns
****
****

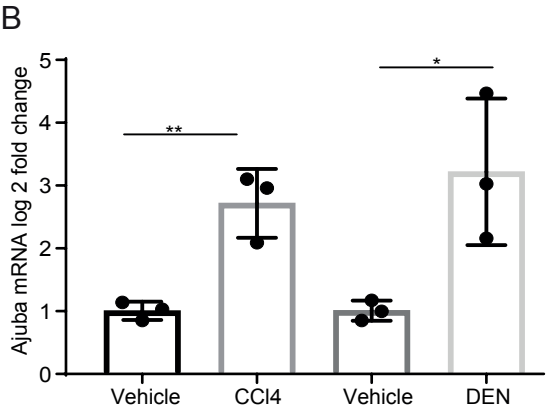
B
Ajuba mRNA log 2 fold change
Vehicle
CCl4
Vehicle
DEN
**
*

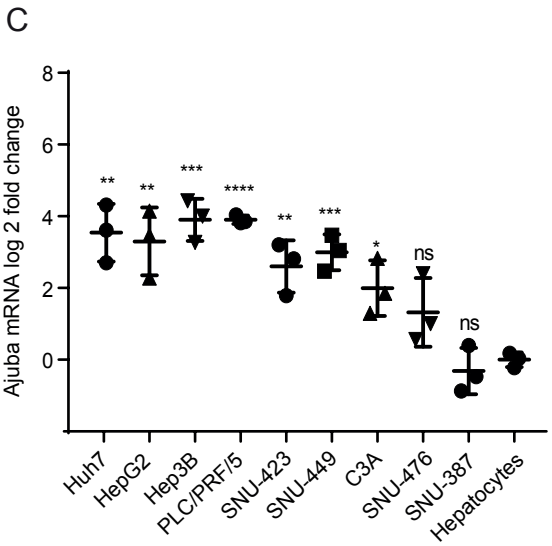
C
Ajuba mRNA log 2 fold change
Huh7
HepG2
Hep3B
PLC/PRF/5
SNU-423
SNU-449
C3A
SNU-476
SNU-387
Hepatocytes

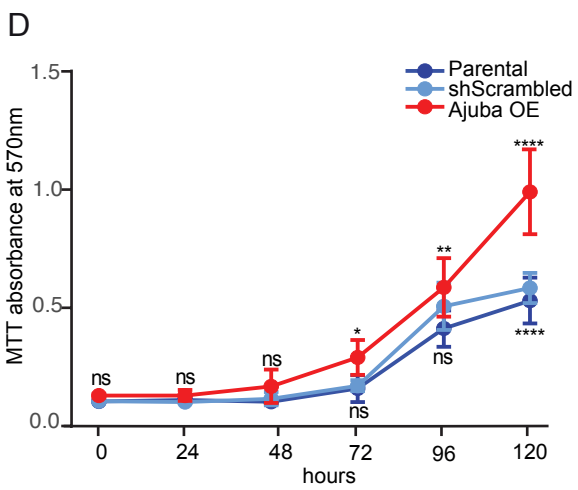
D
MTT absorbance at 570nm
hours
Parental
shScrambled
Ajuba OE

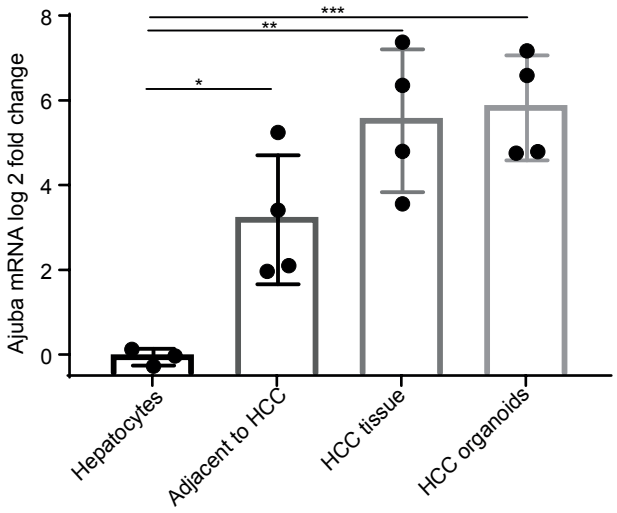
E
Ajuba mRNA log 2 fold change
Hepatocytes
Adjacent to HCC
HCC tissue
HCC organoids

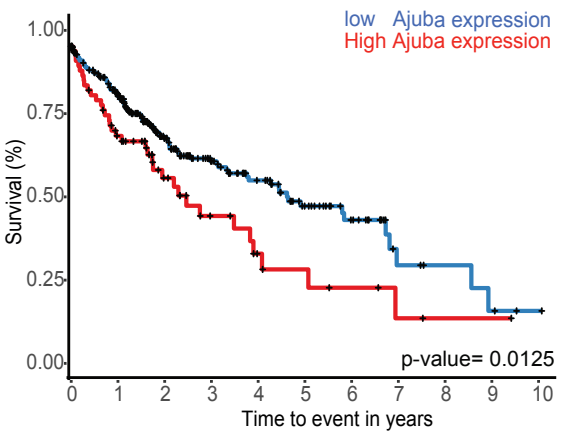
F
low Ajuba expression
High Ajuba expression
Survival (%)
Time to event in years
p-value= 0.0125

Figure 2

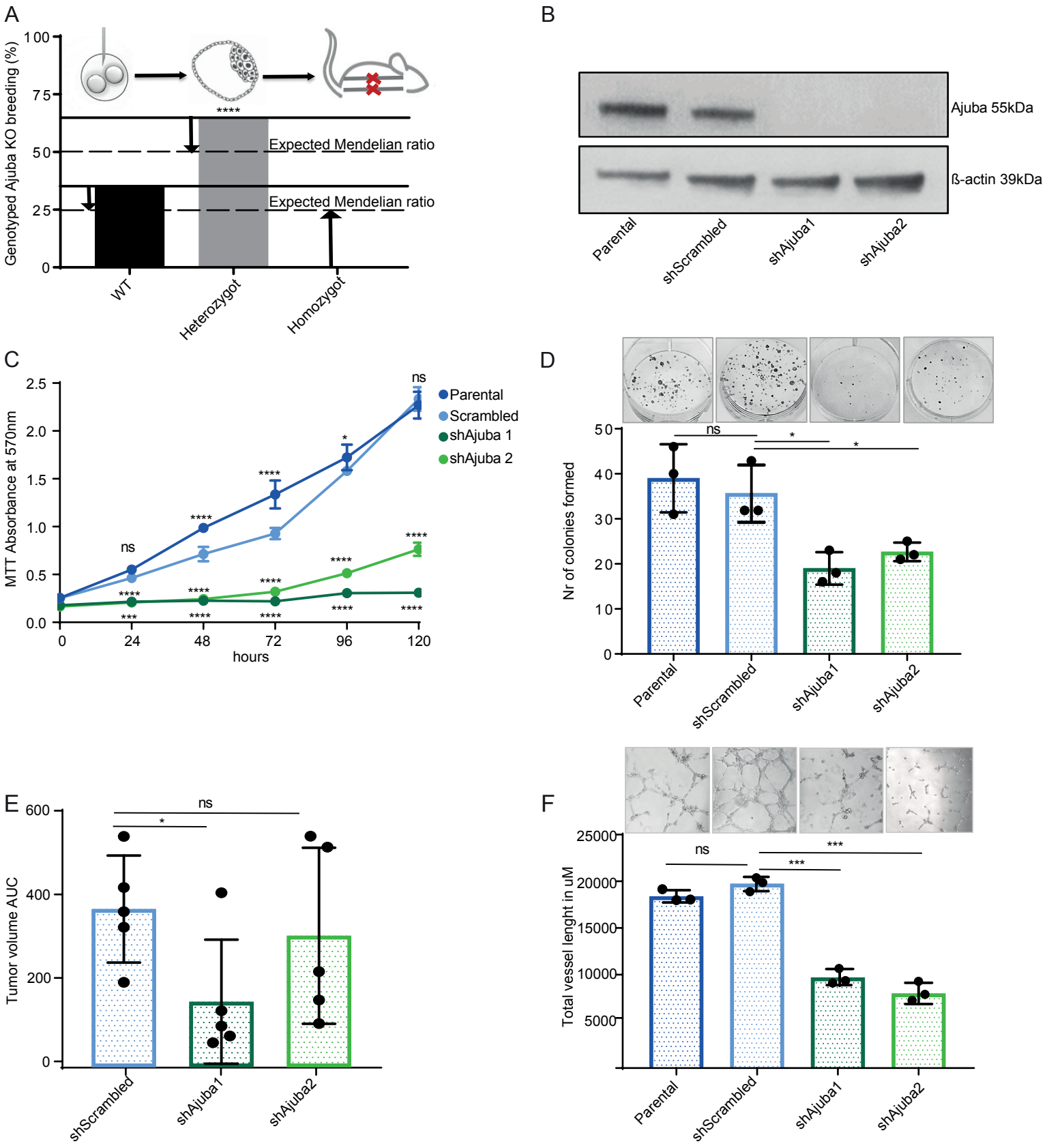
A
Genotyped Ajuba KO breeding (%)
100
75
50
25
0
****
Expected Mendelian ratio
Expected Mendelian ratio
WT
Heterozygot
Homozygot
B
Ajuba 55kDa
ß-actin 39kDa
Parental
shScrambled
shAjuba1
shAjuba2
C
MTT Absorbance at 570nm
2.5
2.0
1.5
1.0
0.5
0.0
0
24
48
72
96
120
hours
ns
Parental
Scrambled
shAjuba 1
shAjuba 2
D
Nr of colonies formed
50
40
30
20
10
0
ns
*
*
Parental
shScrambled
shAjuba1
shAjuba2
E
Tumor volume AUC
600
400
200
0
ns
*
shScrambled
shAjuba1
shAjuba2
F
Total vessel lenght in uM
25000
20000
15000
10000
5000
ns
***
***
Parental
shScrambled
shAjuba1
shAjuba2

Figure 3

A

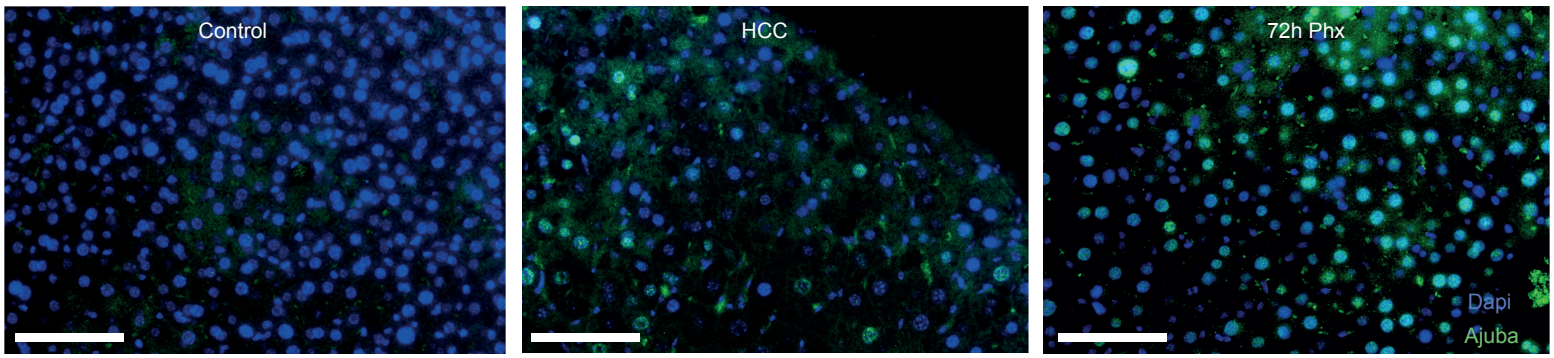
Control
HCC
72h Phx
Dapi
Ajuba

B

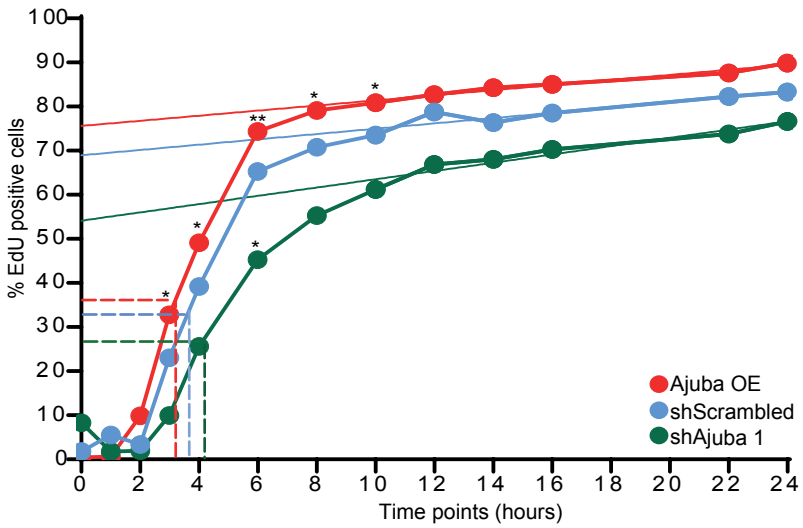
% EdU positive cells
Time points (hours)
Ajuba OE
shScrambled
shAjuba 1

C

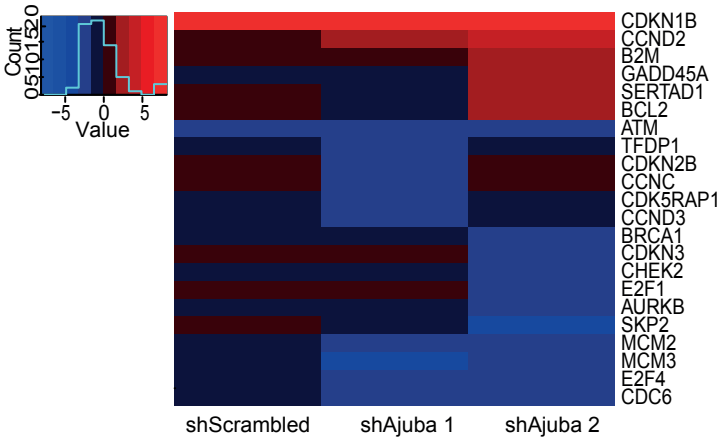
Count
Value
CDKN1B
CCND2
B2M
GADD45A
SERTAD1
BCL2
ATM
TFDP1
CDKN2B
CCNC
CDK5RAP1
CCND3
BRCA1
CDKN3
CHEK2
E2F1
AURKB
SKP2
MCM2
MCM3
E2F4
CDC6
shScrambled
shAjuba 1
shAjuba 2

Figure 4

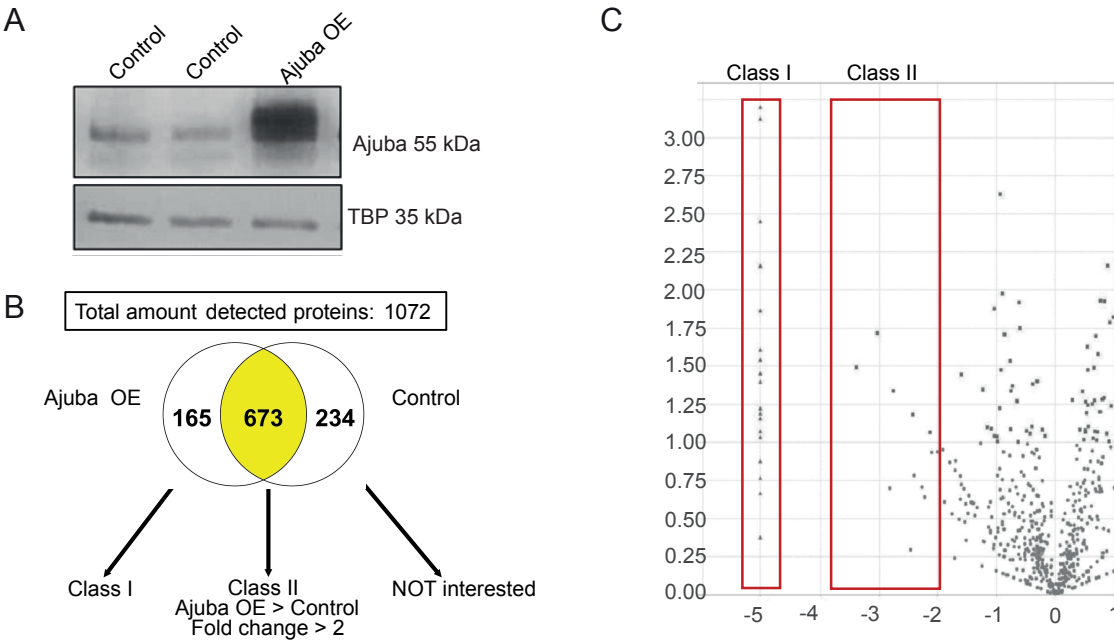
A
Control
Control
Ajuba OE
Ajuba 55 kDa
TBP 35 kDa
B
Total amount detected proteins: 1072
Ajuba OE
165
673
234
Control
Class I
Class II
Ajuba OE > Control
Fold change > 2
NOT interested
C
Class I
Class II
3.00
2.75
2.50
2.25
2.00
1.75
1.50
1.25
1.00
0.75
0.50
0.25
0.00
-5
-4
-3
-2
-1
0
1
2
3
4
5

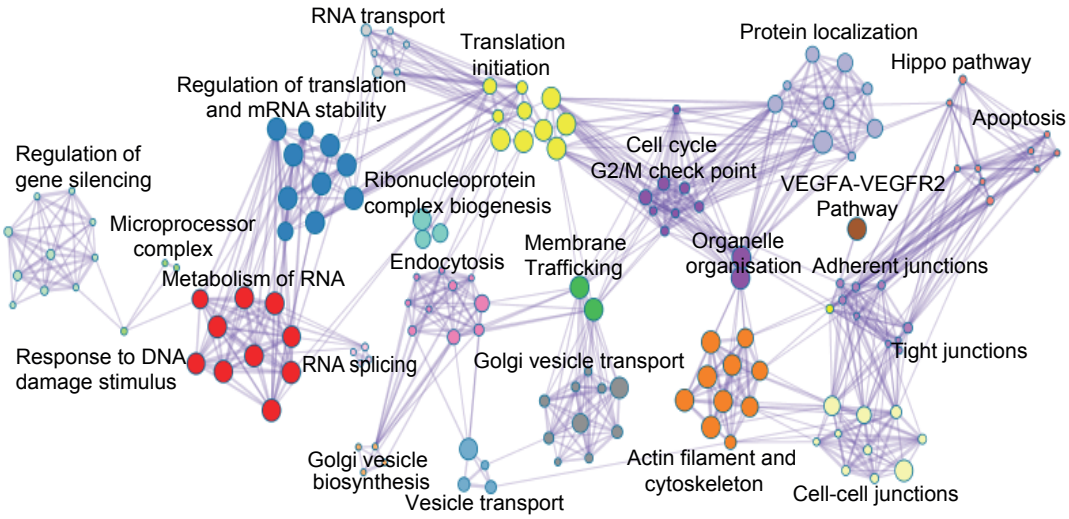
D
RNA transport
Translation initiation
Protein localization
Hippo pathway
Regulation of translation and mRNA stability
Apoptosis
Regulation of gene silencing
Cell cycle G2/M check point
Ribonucleoprotein complex biogenesis
VEGFA-VEGFR2 Pathway
Microprocessor complex
Membrane Trafficking
Organelle organisation
Endocytosis
Adherent junctions
Metabolism of RNA
Tight junctions
Response to DNA damage stimulus
RNA splicing
Golgi vesicle transport
Golgi vesicle biosynthesis
Actin filament and cytoskeleton
Vesicle transport
Cell-cell junctions

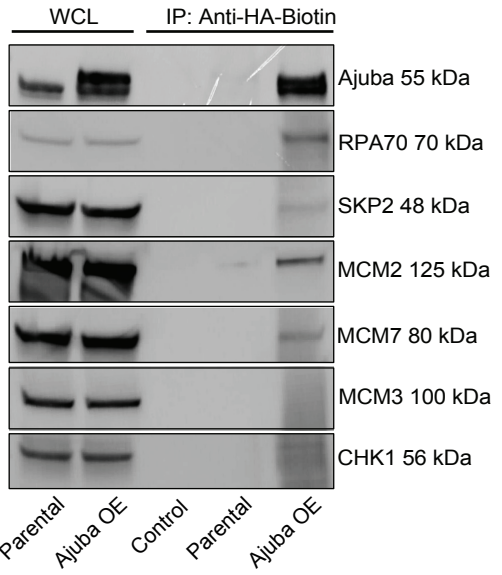
E
WCL
IP: Anti-HA-Biotin
Ajuba 55 kDa
RPA70 70 kDa
SKP2 48 kDa
MCM2 125 kDa
MCM7 80 kDa
MCM3 100 kDa
CHK1 56 kDa
Parental
Ajuba OE
Control
Parental
Ajuba OE

Figure 5

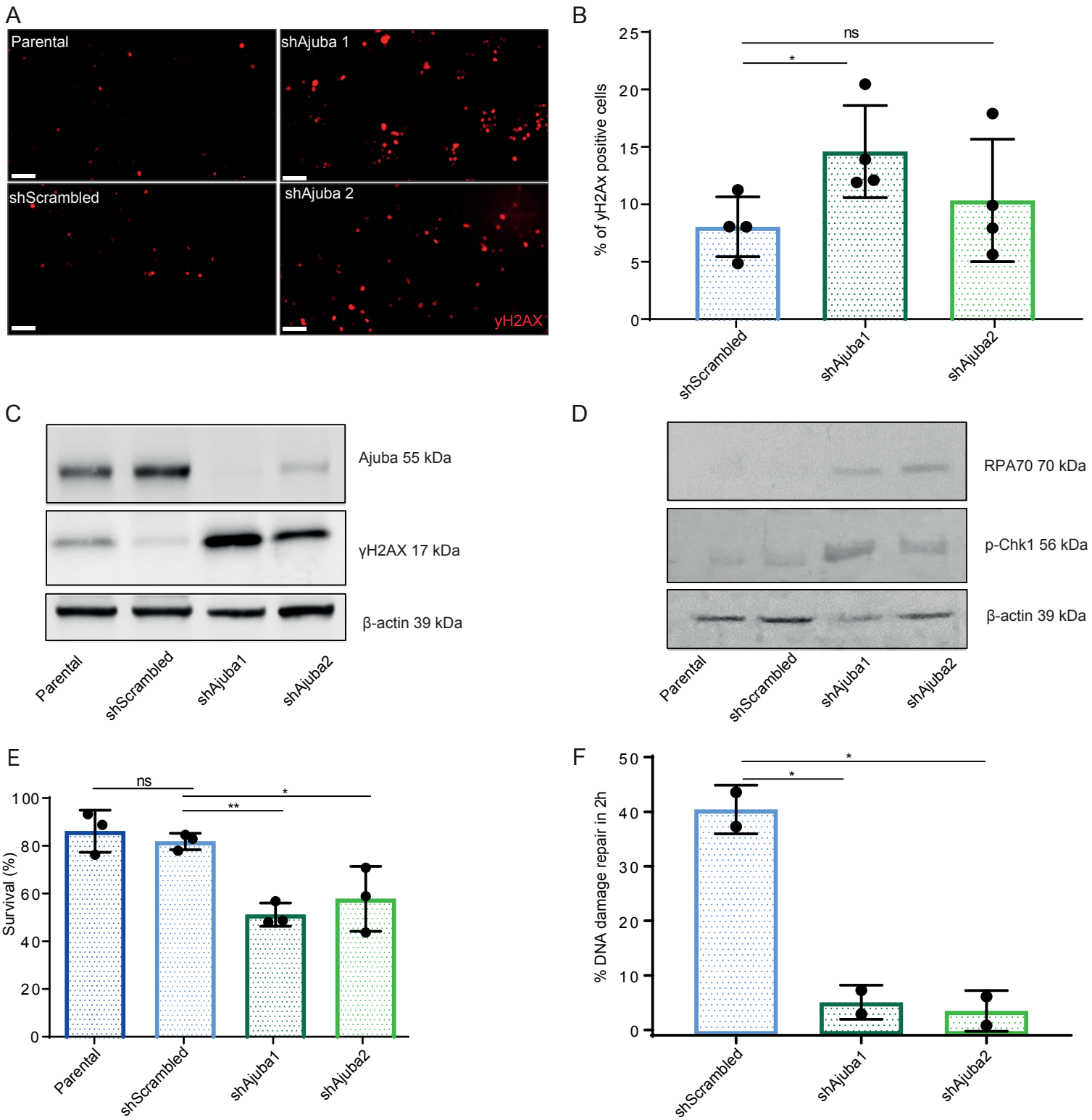
A
Parental
shAjuba 1
shScrambled
shAjuba 2
yH2AX
B
% of yH2Ax positive cells
ns
*
shScrambled
shAjuba1
shAjuba2
C
Ajuba 55 kDa
γH2AX 17 kDa
β-actin 39 kDa
Parental
shScrambled
shAjuba1
shAjuba2
D
RPA70 70 kDa
p-Chk1 56 kDa
β-actin 39 kDa
Parental
shScrambled
shAjuba1
shAjuba2
E
Survival (%)
ns
*
**
Parental
shScrambled
shAjuba1
shAjuba2
F
% DNA damage repair in 2h
*
*
shScrambled
shAjuba1
shAjuba2